

# Geophysical Research Letters<sup>®</sup>

## RESEARCH LETTER

10.1029/2025GL114929

## Methanethiol Abundance and Oxidation in a Polluted Marine Atmosphere



### Key Points:

- Measurements confirm that methanethiol is prevalent at typically 5–25 ppt at a coastal site in UK
- Mixing ratios are higher when winds are from the ocean and at night, likely due to ocean emissions and daytime OH oxidation
- Box modeling highlights NO<sub>3</sub> as an important oxidant for MeSH and that NO<sub>x</sub> pollution has the potential to decrease the SO<sub>2</sub> yield from MeSH

### Supporting Information:

Supporting Information may be found in the online version of this article.

### Correspondence to:

C. Wohl and D. E. Oram,  
c.wohl@uea.ac.uk;  
d.oram@uea.ac.uk

### Citation:

Wohl, C., Forster, G. L., Edwards, P. M., Suntharalingam, P., & Oram, D. E. (2025). Methanethiol abundance and oxidation in a polluted marine atmosphere. *Geophysical Research Letters*, 52, e2025GL114929. <https://doi.org/10.1029/2025GL114929>

Received 20 JAN 2025

Accepted 4 APR 2025

Charel Wohl<sup>1,2</sup> , Grant L. Forster<sup>1,2</sup>, Pete M. Edwards<sup>3,4</sup>, Parvatha Suntharalingam<sup>1</sup> , and David E. Oram<sup>1,2</sup> 

<sup>1</sup>Centre of Ocean and Atmospheric Sciences, School of Environmental Sciences, University of East Anglia, Norwich, UK,

<sup>2</sup>National Center for Atmospheric Science, University of East Anglia, Norwich, UK, <sup>3</sup>Wolfson Atmospheric Chemistry Laboratories, Department of Chemistry, University of York, York, UK, <sup>4</sup>National Center for Atmospheric Science, University of York, York, UK

**Abstract** Biological activity in the surface ocean leads to emissions of methanethiol (MeSH) and dimethyl sulfide (DMS). Measurements of MeSH in the marine atmosphere are sparse and the impact of NO<sub>x</sub> pollution on MeSH oxidation remains unexplored. We present measurements of MeSH and DMS at a coastal site with NO<sub>x</sub> up to 24.3 ppb in the United Kingdom during May and June. Winds coming from the seaward (northerly) direction showed a median (25th quantiles) MeSH mixing ratio of 15.7 (7.9–26.9) ppt. The measurements reveal significantly lower MeSH during daytime. Atmospheric box model calculations suggest that ~25% of the MeSH oxidation is initiated by NO<sub>3</sub> at this site and that NO<sub>x</sub> pollution can reduce the SO<sub>2</sub> yield from MeSH. This work is further evidence for the prevalence of MeSH and illustrates the impact of NO<sub>x</sub> pollution on MeSH oxidation with associated implications for its role in aerosol-cloud processes, and climate.

**Plain Language Summary** The oceans emit substantial amounts of volatile, gaseous sulfur in the form of methanethiol and DMS. Methanethiol measurements in marine air are very sparse, partly because it is hard to measure. Methanethiol is of interest, because it very efficiently reacts in the atmosphere to form SO<sub>2</sub> at a close to 100% yield. SO<sub>2</sub> is a particle forming sulfur gas, cooling the climate. We measured methanethiol in air on the UK coast and found it to be present at 10–30 ppt, a tiny fraction of the molecules in air. We find higher mixing ratios when the winds are from the sea, likely because the oceans are emitting this compound. We also find higher mixing ratios at night, probably due to removal processes initiated by sunlight and physical processes in the atmosphere. Using a computer model, we calculate that nitrogen oxides from shipping exhausts and terrestrial combustion sources can react with methanethiol at night. They have the potential to decrease the efficiency of SO<sub>2</sub> production from methanethiol down to a yield of less than 50%. This case study gives a better appreciation of methanethiol's climatic impact and how this might be different in a polluted marine atmosphere.

## 1. Introduction

Oceanic plankton produces volatile sulfur compounds in the form of methanethiol (MeSH) and dimethyl sulfide (DMS), which ventilate to the atmosphere (Novak et al., 2022). These compounds play a crucial role in cooling the planet by forming SO<sub>2</sub> which contributes to aerosol that seed and/or brighten clouds, thus offsetting much of the anthropogenic warming (Fung et al., 2022; Intergovernmental Panel on Climate Change, 2023). Over the last 40 years, DMS has received all the attention as the main oceanic sulfur compound (Hulswar et al., 2022). New instrumentation and recent measurements in key locations (Gros et al., 2023) highlight that MeSH has a hitherto overlooked impact on climate due to its substantial ocean emissions, fast oxidation and high SO<sub>2</sub> yield (Wohl et al., 2024) thus changing the pre-industrial baseline assumed for many climate change model simulations.

MeSH and DMS have a common precursor, dimethylsulfoniopropionate (DMSP), produced in the surface ocean by the planktonic food web (Hopkins et al., 2023; Kiene & Linn, 2000). Due to rapid biological consumption of MeSH (Kiene, 1996), the standing stock and thus ocean emission of MeSH is about 5 times smaller than that of DMS, with large spatial variations in this ratio (Kettle et al., 2001; Kilgour et al., 2022). Observations of MeSH in the marine atmosphere remain very sparse, but are of high value, toward improved characterization of atmospheric chemical processing and for associated model validation.

In the atmosphere, MeSH is oxidized by hydroxyl radical (OH) or NO<sub>3</sub> to form the methyl thyl radical (CH<sub>3</sub>S) (Butkovskaya & Setser, 2021; Jensen et al., 1992) likely at a 1:1 yield (Novak et al., 2022). The reactions of CH<sub>3</sub>S

© 2025. The Author(s).

This is an open access article under the terms of the [Creative Commons Attribution License](https://creativecommons.org/licenses/by/4.0/), which permits use, distribution and reproduction in any medium, provided the original work is properly cited.



(3/8" o.d., 0.062 wall, opaque cover, only PFA fittings, strictly avoiding any metal). This was used to sample air from the roof of WAO (5 m above ground, approx. 20 m above sea level). The air inlet consisted of a downward facing 90° PFA elbow. Two pumps were used to create a flow of 35 dm<sup>3</sup> min<sup>-1</sup> down the main inlet line. The Vocus subsampled orthogonally from this main flow at a rate of 5 dm<sup>3</sup> min<sup>-1</sup>, where 90–100 cm<sup>3</sup> min<sup>-1</sup> entered the instrument.

Data acquisition was split between measuring zero air hourly from a zero air generator (Vocus PTR Clean Air System, Tofwerk AG) and a calibration gas standard containing DMS every 2 hr. Peak fitting and integration was completed in Tofware v4.0.1 and data files were averaged to 10 s. Zero air was used as a blank for DMS and MeSH. DMS was quantified by interpolating the sensitivity derived from the calibration gas standard. MeSH was not present in the calibration gas standard used here. It has been reported to react on metal surfaces such as a regulator, to form dimethyl disulfide (Perraud et al., 2016). Instead, MeSH was quantified in the field using the internal calibration curve of the instrument and mimicking the sensitivity changes observed from DMS. The internal calibration curve of the instrument relies on a relationship between sensitivity and the reaction rate with H<sub>3</sub>O<sup>+</sup> derived in the field using the suite of calibrants in the gas standard (Figure S2 in Supporting Information S1). We used a liquid calibration unit (LCU, Tofwerk AG) in the laboratory prior to deployment to confirm that MeSH follows this relationship (Figure S3 in Supporting Information S1). A liquid standard of MeSH for LCU analysis was prepared by dissolving sodium methanethiolate in water. We used a  $k_{\text{PTR}}$  of  $1.8 \times 10^{-9}$  cm<sup>3</sup> s<sup>-1</sup> as determined from experimental studies (Williams et al., 1998). Overall, we estimate that our DMS and MeSH measurements have an error of 5% and 15% respectively (Text S1 in Supporting Information S1).

### 2.3. Atmospheric Chemical Box Model

An atmospheric chemistry 0-D chemical box model was developed by modifying the MCM v3.3.1 (Jenkin et al., 1997; Saunders et al., 2003) run in the Framework for 0-D Atmospheric Modeling (FOAM) (Wolfe et al., 2016). The mechanism for DMS, CH<sub>4</sub> and C<sub>5</sub>H<sub>8</sub> (isoprene) was downloaded from the MCM website (<http://mcm.york.ac.uk>, last accessed 15/01/2025). We modified reaction rate constants and added reactions of DMS oxidation as per recommendations by Jacob et al. (2024) focusing only on pathways relevant to MeSH oxidation. We added oxidation of MeSH by OH and NO<sub>3</sub> to form CH<sub>3</sub>S (Burkholder et al., 2019; Butkovskaya & Setser, 2021; Jensen et al., 1992). There are other oxidants of MeSH (e.g., BrO, Cl, HO<sub>2</sub>), but these reactions are poorly studied and we lack constraint data at this site, which precludes reliable atmospheric modeling (Burkholder et al., 2019). Reactions updated over the standard MCM DMS mechanism are provided in the supplement (Table S1 in Supporting Information S1).

Although a concurrent comprehensive chemical supporting observational data set is not available, the well characterized nature of the WAO site means historical data is available to provide sufficient constraints for the purpose of assessing MeSH loss mechanisms at this location. Campaign mean observed values for northerly winds (315°North East (NE)–45°North West (NW)) of meteorological parameters, that is, pressure (1,012.52 mbar), temperature (285 K) and relative humidity (87%) were provided by the station and prescribed in the model. Similarly, fixed mixing ratios of CO (130 ppb) and CH<sub>4</sub> (2,100 ppb) were used which corresponds to typical observed values during northerly winds for the campaign. We used fixed mixing ratio values of 522 ppb hydrogen (Forster et al., 2012), 0.05 ppb HNO<sub>3</sub> (Bannan et al., 2017) and 10 ppt isoprene (Phillips et al., 2021). The first-order rate constant for physical dilution out of the boundary layer was set to one per day. Due to a lack of comprehensive volatile organic compounds observations, we prescribed model OH to simulate DMS and MeSH oxidation. The OH diurnal cycle was set to mirror the observed solar radiation cycle with a maximum at  $4 \times 10^6$  cm<sup>-3</sup> (Figure S5a in Supporting Information S1), based on previous observations at this site by Woodward-Massey et al. (2023). Ozone mixing ratios were prescribed by using the observed diurnally varying hourly mean during northerly winds (Figure S5b in Supporting Information S1). The model was set to conserve NO<sub>x</sub> (= NO + NO<sub>2</sub> = constant) and jcorr factor was adjusted to 0.4 (Wolfe et al., 2016) to yield approximately the measured NO to NO<sub>2</sub> ratio (Figure S5c in Supporting Information S1). The products of MeSH oxidation were labeled in the box model. The model was allowed to spin up for 4 days and data from the 5th day is presented here.

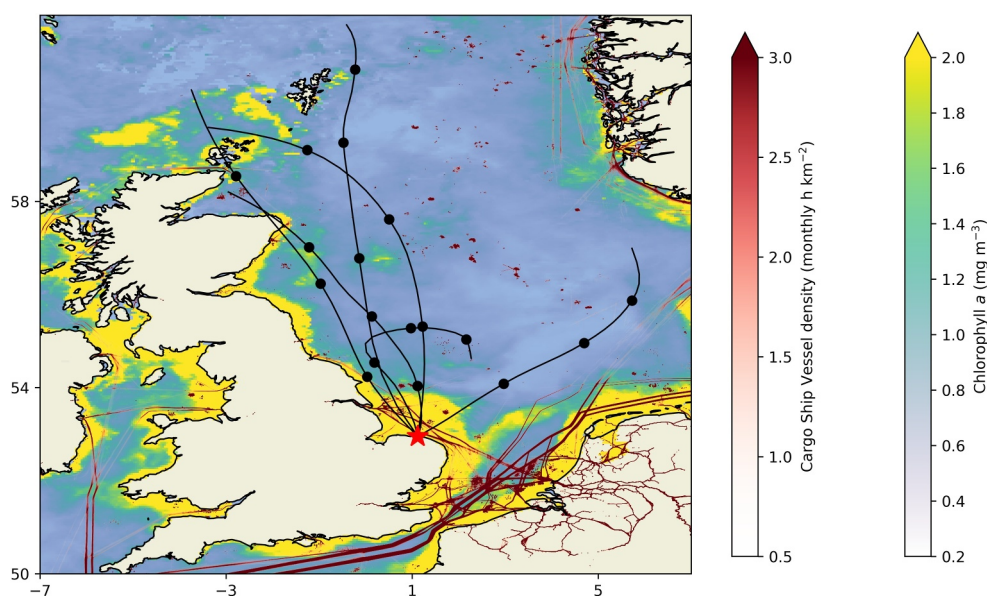


**Figure 2.** Back trajectories for northerly wind episodes. Representative air mass back trajectories for 24 hr indicated as solid black lines with markers denoting 6 hr intervals. Overlaid on a map of Chl *a* (MODIS monthly June 2024) and Cargo Ship Vessel Density (June 2024). Location of WAO indicated as a red star.

### 3. Observations

#### 3.1. Environmental Setting

For the time period of the campaign, the wind direction showed a bimodal distribution of either coming from the southwest (defined here as 180°W–270°S) or from a northerly direction (defined here as 315°NE–45°NW), which highly influenced mixing ratios and variability of trace gases (Figure S6 and Text S2 in Supporting Information S1). During northerly winds, the NO<sub>2</sub> mixing ratio distribution is highly skewed and influenced by high mixing ratio events (northerly winds NO<sub>2</sub>, mean: 1.68 ppb, median 0.99 ppb). We observe episodes of around 10 ppb NO<sub>x</sub> coinciding with peaks in black carbon (particularly around 21/05 and 01/06, Figure S6 in Supporting Information S1), flagging these as very local combustion pollution events, likely from shipping emissions. These events also coincide with drops in ozone (O<sub>3</sub>) of about 10 ppb. Shipping related NO<sub>x</sub> has been shown to reduce O<sub>3</sub> in this region at this time of year (Jonson et al., 2020). These events are also accompanied by relatively small peaks in CO<sub>2</sub>, CO and CH<sub>4</sub>. Shipping emissions are expected to emit these gases (Yi et al., 2024). Satellite tropospheric column NO<sub>2</sub> (Figure S4 in Supporting Information S1) suggests that northerly air episodes may also be impacted by continental outflow from terrestrial NO<sub>x</sub> emissions.

Air mass back trajectories for some northerly winds/marine air episodes are overlaid on distributions of chlorophyll *a* (Chl *a*) and Cargo Ship Vessel density in Figure 2.

The air mass back trajectories indicate that northerly air masses have predominantly traveled over the ocean in the day preceding arrival at WAO, but they are not purely marine air masses and likely picked up some terrestrial influence. This is supported by the measurements of atmosphere radon activity (<sup>222</sup>Rn), which show a median of 603.5 mBq m<sup>-3</sup> in air arriving from the north. By comparison, previous work by Fleming (2023) used a threshold of less than 200 mBq m<sup>-3</sup> to identify marine dominated airmasses at this site. The MODIS Chl *a* data for June 2024 highlights that the Chl *a* concentration is between 0.5–1 mg m<sup>-3</sup>, indicating moderate biological activity during the measurement period. The Cargo Ship density map highlights a shipping lane north of the observatory. Note that the map only includes cargo ship vessel density and thus likely represents an underestimate of the true vessel abundance. Areas with higher cargo vessel density in the North Sea are probably related to oil platforms. This map highlights that northerly air episodes were influenced by a variety of emissions from both marine biological and anthropogenic sources.

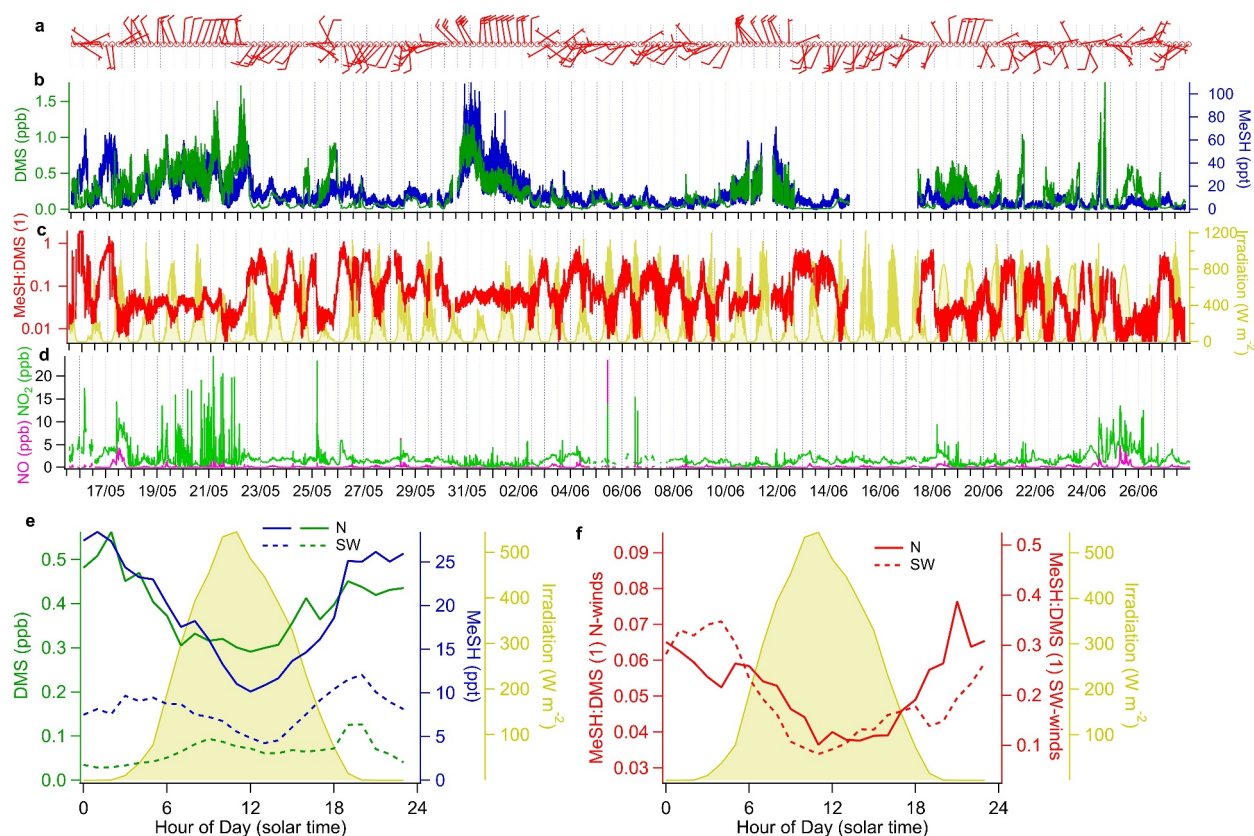


**Figure 3.** Dimethyl sulfide (DMS) and MeSH mixing ratios (a) Wind Barbs. Short wind barb 5 kts. Shafts pointing to the direction from which the wind is blowing. North = ocean (b) Measured DMS and methanethiol (MeSH) mixing ratios. (c) MeSH:DMS ratio and irradiance. (d)  $\text{NO}_x$  measurements (e) Hourly mean MeSH and DMS mixing ratio separated by wind direction, plotted with the mean irradiance profile (f) Mean MeSH:DMS ratio depending on wind direction and mean irradiance profile.

### 3.2. Methanethiol and Dimethyl Sulfide Mixing Ratios

The campaign time series of MeSH and DMS air mixing ratios and  $\text{NO}_x$  is presented in Figures 3b and 3c.

The campaign mean, median and inter-quantile range of MeSH was 12.3, 8.6 and 4.7–15.1 ppt (volume mixing ratio - here and throughout), while the mean, median and inter-quantile range of DMS was 0.197, 0.106 and 0.034–0.294 ppb. For winds from a northerly direction, the mean MeSH mixing ratio was 19.0 ppt, while the median and inter-quantile range was 15.7 and 7.9–26.9 ppt. During northerly winds, the mean, median and inter quantile range of DMS was 0.382, 0.333 and 0.213–0.517 ppb. These methanethiol mixing ratios are similar to previous observations in marine air in the Eastern North Atlantic (Kilgour et al., 2024), Eastern Pacific (Novak et al., 2022) or the Southwest Pacific Ocean (Lawson et al., 2020), but higher than measurements over the Southern Ocean (Berresheim, 1987). The DMS mixing ratios measured in marine air during this campaign are similar to other measurements in spring/summer on the west coast of the UK (Phillips et al., 2021; Yang et al., 2013). The campaign mean, median and inter-quantile range of MeSH:DMS ratio was 0.140, 0.071 and 0.036–0.173. This is comparable to previous observations and provides further evidence that MeSH is present in the atmosphere at mixing ratios of about 5%–15% that of DMS. Overall, these measurements confirm that MeSH accumulates in the lower troposphere to substantial amounts, despite a relatively short lifetime, estimated as 0.125–0.4 days in a box model (Lawson et al., 2020; Novak et al., 2022) and 1.5 days (Wohl et al., 2024) in a chemistry-climate model.

We find that MeSH and DMS display significant diurnal variability (Figures 3e and 3f). For northerly winds, the average MeSH mixing ratio during the day is 16.5 ppt, but 26.2 ppt during the night ( $t$  test,  $n_{\text{day}} = 16$ ;  $n_{\text{night}} = 8$ ;  $t$  stat =  $-7.6$ ;  $t$  critical = 2.0;  $p = 0.01$ ). Similarly, during northerly winds, the mean DMS daytime mixing ratio was 0.356 ppb, while at night it was 0.466 ppb ( $t$  test,  $n_{\text{day}} = 16$ ;  $n_{\text{night}} = 8$ ;  $t$  stat =  $-4.9$ ;  $t$  critical = 2.1;  $p = 0.01$ ). The MeSH:DMS ratio during northerly winds is also lower during the day than at night. The reaction of MeSH

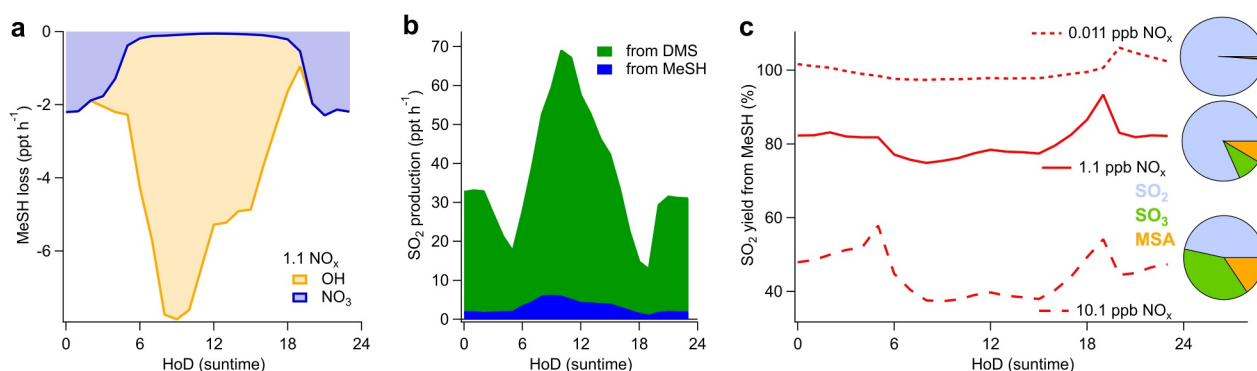


**Figure 4.** Box modeling the oxidative fate of MeSH. (a) Stacked MeSH loss rates (b) stacked  $\text{SO}_2$  production rates from MeSH and DMS (c)  $\text{SO}_2$  yield from MeSH during hours of the day under different  $\text{NO}_x$  conditions. Pie chart inserts show the average MeSH oxidation product distribution under different  $\text{NO}_x$ .

with OH is about 5–10 times faster than DMS with OH (Burkholder et al., 2019; Lawson et al., 2020). Assuming a constant emission, the lower MeSH:DMS ratio during the day suggests that daytime oxidation is driving much of this diurnal variability owing to the faster reaction of OH with MeSH than with DMS. Although boundary layer height changes could also play a role in this diel cycle. All of the previous campaigns investigating MeSH and DMS in air have found that MeSH and DMS mixing ratios vary diurnally in the marine atmosphere, with the relative change being consistently larger for MeSH than for DMS (Deng et al., 2024; Kilgour et al., 2024; Lawson et al., 2020; Novak et al., 2022). This significant diurnal variability is an important factor to consider for model to observation comparisons.

MeSH and DMS show remarkable co-variation. During northerly winds, MeSH and DMS significantly correlate ( $P = 0.000$ ,  $N = 81,065$ , slope 46.5 ppt/ppb, intercept 1.2 ppt) giving an  $R^2$  value of 0.56. In marine air, Novak et al. (2022), Kilgour et al. (2024, 2025) found an  $R^2$  of 0.61, 0.60 and 0.56 respectively, while in Lawson et al. (2020) the  $R^2$  is 0.3 using all data. This supports the premise that MeSH and DMS have common sources in the marine atmosphere, namely DMSP breakdown in seawater and wind driven co-emission of DMS and MeSH (Kiene, 1996; Hopkins et al., 2023). During winds coming from the southwest, MeSH and DMS also correlate significantly ( $P = 0.000$ ,  $N = 99,876$ ) and with a similar slope and intercept (slope 42.1 ppt/ppb, intercept 5.8 ppt), but with a much lower  $R^2$  of 0.20. This suggests that terrestrial sources of MeSH and DMS are more distinct leading to decoupling of both compounds' mixing ratios. For example, MeSH is emitted from a variety of human activities, for example, from waste management, and has some specific industrial applications, for example, a gas odorant for natural gas (Bayout et al., 2023). Some measurements in urban areas find episodically very high MeSH (Deng et al., 2024; Susaya et al., 2011). Emissions from these potentially close-by anthropogenic sources could explain the poorer correlation between MeSH and DMS during the south-westerly winds.

#### 4. Oxidative Fate of MeSH in the Polluted Atmosphere

We explore the atmospheric fate of MeSH using a box model constrained with measured, diurnally varying mixing ratios of MeSH, DMS and other atmospheric components for northerly, seaward winds (as described in Sect. 2.3). From constrained OH and modeled  $\text{NO}_3$ , the loss rate of MeSH and the resulting  $\text{SO}_2$  production rate and yield is calculated. The sensitivity of the distribution of MeSH oxidation products is tested by varying the  $\text{NO}_x$  mixing ratio, using the range encountered during the deployment. To estimate the sensitivity to  $\text{NO}_x$ , the  $\text{NO}_x$  mixing ratio is changed to 0.011 (pristine), 1.1 (similar to WAO median) and 10.1 ppb (moderate  $\text{NO}_x$ , ship exhaust plumes).

Using this setup, we model  $\sim 1$  ppt  $\text{NO}_3$  (Figure S5a in Supporting Information S1) (previous observations at WAO 0–10 ppt (Carslaw et al., 1997)) and radical mixing ratios of up to  $\sim 20$  ppt (Figure S5d in Supporting Information S1) (previous observations at WAO up to 24 ppt (Woodward-Massey et al., 2023)).

The MeSH loss rate (Figure 4a) displays strong diurnal variability, peaking at mid-day due to OH oxidation, which explains in part the diurnal variability of MeSH in the atmosphere (Figure 3d). Under these atmospheric conditions, diurnally averaged, three quarters of MeSH is oxidized by OH during the day and one quarter by  $\text{NO}_3$  at night, though this ratio is sensitive to the oxidants in the model. The bimolecular rate constant of MeSH with

$\text{NO}_3$  is  $0.89 \times 10^{-12} \text{ cm}^3 \text{ molecule}^{-1} \text{ s}^{-1}$  at 298 K, while it is  $1.09 \times 10^{-12} \text{ cm}^3 \text{ molecule}^{-1} \text{ s}^{-1}$  at 298 K for DMS with  $\text{NO}_3$ . This gives a lifetime of MeSH and DMS to  $\text{NO}_3$  oxidation of 12 and 10 hr respectively (for  $\text{NO}_3 = 1 \text{ ppt}$  and mean measured nighttime MeSH and DMS). This illustrates that MeSH oxidation by  $\text{NO}_3$  in the polluted atmosphere is an important process that has previously been overlooked.

Figure 4b shows that some of the  $\text{SO}_2$  from MeSH and DMS is produced at night in the box model due to oxidation initiated by  $\text{NO}_3$ . Thus nitrogen oxides change the time of day of  $\text{SO}_2$  production compared to more pristine conditions. Accounting for MeSH oxidation increases the  $\text{SO}_2$  production rate by 8%, over only accounting for DMS. This illustrates that MeSH makes a substantial contribution to production of natural background marine  $\text{SO}_2$  at this site.

For 1.1 ppb of  $\text{NO}_x$ , close to the median condition encountered during this campaign, we calculate a mean MeSH to  $\text{SO}_2$  yield of 81% (Figure 4c). Thus under these conditions, 9% of the MeSH is converted to MSA and 10% to  $\text{SO}_3$ , as indicated by the pie chart insert (Figure 4c). After reducing  $\text{NO}_x$  to 0.011 ppb, we calculate a MeSH to  $\text{SO}_2$  yield of 99% (Figure 4c). This confirms that under low  $\text{NO}_x$ , the MeSH to  $\text{SO}_2$  yield remains at near 1:1, backed by calculations in Novak et al. (2022) and Chen et al. (2021). Running the model at 10.1 ppb  $\text{NO}_x$ , representative of the ship plumes or continental outflow regions, we find that the MeSH to  $\text{SO}_2$  yield decreases to 45%, yielding 36% as  $\text{SO}_3$  and 15% as MSA (Figure 4c) and the remainder as other stable intermediates. Under low  $\text{NO}_x$ , most of the  $\text{SO}_2$  from MeSH is produced from the reaction of  $\text{CH}_3\text{SO}$  with  $\text{O}_3$  and to a lesser extent the decomposition of  $\text{CH}_3\text{SOO}$  (Figure 1). Under high  $\text{NO}_x$ ,  $\text{SO}_2$  is produced from the decomposition of  $\text{CH}_3\text{SO}_2$  and the reaction from  $\text{CH}_3\text{SO}$  with  $\text{NO}_2$  and  $\text{O}_3$  (Figure 1). Hence, under higher  $\text{NO}_x$ , the sulfur from MeSH is moved further right in the reaction chain in Figure 1 ultimately producing more  $\text{SO}_3$  and MSA from reactions of the  $\text{CH}_3\text{SO}_3$  radical. This can give MeSH a similar  $\text{SO}_2$  yield as DMS (Jacob et al., 2024) in a polluted atmosphere.

It is worth emphasizing that the  $\text{SO}_2$  yield under different  $\text{NO}_x$  conditions has been calculated by varying the  $\text{NO}_x$  mixing ratio only. Comparing this to Figure 1, the MeSH to  $\text{SO}_2$  yield could also be sensitive to  $\text{O}_3$ ,  $\text{HO}_2$  and RH mixing ratios. To test the robustness of our conclusions and lacking concurrent radical measurements for constraint, we varied  $\text{O}_3$  and  $\text{HO}_2$  from 20 to 60 ppb and 10–50 ppt respectively. Keeping  $\text{NO}_x$  at 1.1 ppb and the OH profile constant, the MeSH to  $\text{SO}_2$  yield changed by less than 5%. Our calculations rely on published rate constants surrounding the  $\text{CH}_3\text{SO}_2$  and  $\text{CH}_3\text{SO}_3$  radical, which were found to be highly uncertain by Jacob et al. (2024) and deserve more research. Nevertheless, our calculations robustly highlight that the presence of  $\text{NO}_x$  promotes oxidation pathways producing MSA and  $\text{SO}_3$ , which is not occurring under more pristine conditions. The reactions studied here have been included when assessing the climatic impact of MeSH emissions (Wohl et al., 2024). Hence, the box modeling presented here is a case study, nuancing our understanding of the oxidation of MeSH.

## 5. Conclusions

We present measurements of MeSH and DMS in air at a UK coastal site on the North Sea. Measurements show that MeSH is a prevalent sulfur compound at this site, present 5–25 ppt, typically 5%–15% that of DMS. Mixing ratios of both sulfur compounds are higher during the night than during the day, likely due to daytime oxidation by OH and aided by changes in boundary layer height. Mixing ratios are higher when winds are from the sea than from land, highlighting the ocean as the dominant source of these compounds at this location. Box modeling suggests that the  $\text{NO}_3$  radical is a major oxidant for MeSH, accounting for approximately 25% of MeSH gas phase chemical removal in marine air at this site. The box modeling also shows that  $\text{NO}_x$  pollution substantially reduces the  $\text{SO}_2$  yield from MeSH and shifts the oxidation products of MeSH toward more MSA,  $\text{SO}_3$  and other stable intermediates. While the MeSH to  $\text{SO}_2$  yield is 99% in near-pristine conditions, it decreases to 81% at 1.1 ppb  $\text{NO}_x$  and 45% at 10.1 ppb  $\text{NO}_x$ . These findings have implications for our understanding of the oxidative fate of MeSH in the atmosphere. It also highlights how anthropogenic pollution affects oxidative and climate cooling processes.

## Data Availability Statement

DMS and MeSH mixing ratio data and associated meteorological and trace gas measurements are archived at Wohl (2025).

## Acknowledgments

This work has been supported by the National Centre of Atmospheric Science through the FAAM Mid-Life upgrade. We thank the Atmospheric Measurement and Observation Facility (AMOF), part of the National Centre for Atmospheric Science (NCAS), for its support for the Weybourne Atmospheric Observatory. We thank Alex Etchells (UEA, ITCS) for IT support at WAO and Lorrie Jacob (University of Cambridge) for helpful discussions surrounding the MCM box modeling. The work was supported by the UK Natural Environment Research Council (NERC) CARES project (ConstrAining the ROle of Sulfur in the earth system), NE/W009307/1 and the UK National Center for Atmospheric Sciences (FAAM mid-life upgrade project). The Vocus instrument was funded through a NERC Capital Equipment award (NE/T009020/1).

## References

- Archer-Nicholls, S., Allen, R., Abraham, N. L., Griffiths, P. T., & Archibald, A. T. (2023). Large simulated future changes in the nitrate radical under the CMIP6 SSP scenarios: Implications for oxidation chemistry. *Atmospheric Chemistry and Physics*, 23(10), 5801–5813. <https://doi.org/10.5194/acp-23-5801-2023>
- Bannan, T. J., Bacak, A., Le Breton, M., Flynn, M., Ouyang, B., McLeod, M., et al. (2017). Ground and Airborne U.K. Measurements of Nitryl Chloride: An investigation of the role of Cl Atom oxidation at Weybourne atmospheric observatory. *Journal of Geophysical Research: Atmospheres*, 122(20), 11154–11165. <https://doi.org/10.1002/2017JD026624>
- Barnes, I., Hjorth, J., & Mihalopoulos, N. (2006). Dimethyl sulfide and dimethyl sulfoxide and their oxidation in the atmosphere. *Chemistry Review*, 106(3), 940–975. <https://doi.org/10.1021/cr020529+>
- Bayout, A., Cammarano, C., Costa, I. M., Veryasov, G., & Hulea, V. (2023). Methyl mercaptan production – Catalysts and processes. *Catalysis Science and Technology*, 13(13), 3762–3778. <https://doi.org/10.1039/D3CY00384A>
- Berresheim, H. (1987). Biogenic sulfur emissions from the Subantarctic and Antarctic Oceans. *Journal of Geophysical Research*, 92(D11), 13245–13262. <https://doi.org/10.1029/JD092iD11p13245>
- Burkholder, J. B., Sander, S. P., Abbatt, J. P. D., Barker, J. R., Cappa, C. D., Crouse, J. D., et al. (2019). Chemical kinetics and photochemical data for use in atmospheric studies. *Evaluation No. 19*. <http://jpldataeval.jpl.nasa.gov>
- Butkovskaya, N. I., & Setser, D. W. (2021). Reactions of OH and OD radicals with simple thiols and sulfides studied by infrared chemiluminescence of isotopic water products: Reaction OH + CH<sub>3</sub>SH revisited. *International Journal of Chemical Kinetics*, 53(6), 702–715. <https://doi.org/10.1002/kin.21475>
- Carlaw, N., Carpenter, L. J., Plane, J. M. C., Allan, B. J., Burgess, R. A., Clemitshaw, K. C., et al. (1997). Simultaneous observations of nitrate and peroxy radicals in the marine boundary layer. *Journal of Geophysical Research*, 102(D15), 18917–18933. <https://doi.org/10.1029/97JD00399>
- Chen, J., Berndt, T., Möller, K. H., Lane, J. R., & Kjaergaard, H. G. (2021). Atmospheric fate of the CH<sub>3</sub>SOO radical from the CH<sub>3</sub>S + O<sub>2</sub> equilibrium. *Journal of Physical Chemistry A*, 125(40), 8933–8941. <https://doi.org/10.1021/acs.jpca.1c06900>
- Curran, M. A. J., van Ommen, T. D., Morgan, V. I., Phillips, K. L., & Palmer, A. S. (2003). Ice core evidence for antarctic sea ice decline since the 1950s. *Science*, 302(5648), 1203–1206. <https://doi.org/10.1126/science.1087888>
- Deng, K., Huo, J., Wang, Y., Wang, L., Yin, S., Li, C., et al. (2024). Characteristics of atmospheric reduced-sulfur compounds at a suburban site of Shanghai. *Journal of Environmental Sciences*. <https://doi.org/10.1016/j.jes.2024.06.030>
- Fleming, L. S. (2023). Analyses of multi-species greenhouse gases and related tracers using novel measurements at Weybourne Atmospheric Observatory. University of East Anglia. Retrieved from <https://ueaeprints.uea.ac.uk/id/eprint/94364>
- Forster, G. L., Sturges, W. T., Fleming, Z. L., Bandy, B. J., & Emeis, S. (2012). A year of H<sub>2</sub> measurements at Weybourne atmospheric observatory, UK. *Tellus B: Chemical and Physical Meteorology*, 64(1), 17771. <https://doi.org/10.3402/tellusb.v64i0.17771>
- Fung, K. M., Heald, C. L., Kroll, J. H., Wang, S., Jo, D. S., Gettelman, A., et al. (2022). Exploring dimethyl sulfide (DMS) oxidation and implications for global aerosol radiative forcing. *Atmospheric Chemistry and Physics*, 22(2), 1549–1573. <https://doi.org/10.5194/acp-22-1549-2022>
- Goss, M. B., & Kroll, J. H. (2024). Chamber studies of OH + dimethyl sulfoxide and dimethyl disulfide: Insights into the dimethyl sulfide oxidation mechanism. *Atmospheric Chemistry and Physics*, 24(2), 1299–1314. <https://doi.org/10.5194/acp-24-1299-2024>
- Gros, V., Bonsang, B., Sarda-Estève, R., Nikolopoulos, A., Metfies, K., Wietz, M., & Peeken, I. (2023). Concentrations of dissolved dimethyl sulfide (DMS), methanethiol and other trace gases in context of microbial communities from the temperate Atlantic to the Arctic Ocean. *Bioessences*, 20(4), 851–867. <https://doi.org/10.5194/bg-20-851-2023>
- Hodshire, A. L., Campuzano-Jost, P., Kodros, J. K., Croft, B., Nault, B. A., Schroder, J. C., et al. (2019). The potential role of methanesulfonic acid (MSA) in aerosol formation and growth and the associated radiative forcings. *Atmospheric Chemistry and Physics*, 19(5), 3137–3160. <https://doi.org/10.5194/acp-19-3137-2019>
- Hopkins, F. E., Archer, S. D., Bell, T. G., Suntharalingam, P., & Todd, J. D. (2023). The biogeochemistry of marine dimethylsulfide. *Nature Reviews Earth & Environment*, 4(6), 361–376. <https://doi.org/10.1038/s43017-023-00428-7>
- Hulswar, S., Simó, R., Galí, M., Bell, T. G., Lana, A., Inamdar, S., et al. (2022). Third revision of the global surface seawater dimethyl sulfide climatology (DMS-Rev3). *Earth System Science Data*, 14(7), 2963–2987. <https://doi.org/10.5194/essd-14-2963-2022>
- Intergovernmental Panel on Climate Change (IPCC). (2023). *Climate Change 2021 – The Physical Science Basis: Working Group I Contribution to the Sixth Assessment Report of the Intergovernmental Panel on Climate Change*. Cambridge University Press. Retrieved from <https://www.cambridge.org/core/books/climate-change-2021-the-physical-science-basis/415F29233B8BD19FB55F65E3DC67272B>
- Jacob, L. S. D., Giorio, C., & Archibald, A. T. (2024). Extension, development, and evaluation of the representation of the OH-initiated dimethyl sulfide (DMS) oxidation mechanism in the Master Chemical Mechanism (MCM) v3.3.1 framework. *Atmospheric Chemistry and Physics*, 24(5), 3329–3347. <https://doi.org/10.5194/acp-24-3329-2024>
- Jenkin, M. E., Saunders, S. M., & Pilling, M. J. (1997). The tropospheric degradation of volatile organic compounds: A protocol for mechanism development. *Atmospheric Environment*, 31(1), 81–104. [https://doi.org/10.1016/S1352-2310\(96\)00105-7](https://doi.org/10.1016/S1352-2310(96)00105-7)
- Jensen, N. R., Hjorth, J., Lohse, C., Skov, H., & Restelli, G. (1992). Products and mechanisms of the gas phase reactions of NO<sub>3</sub> with CH<sub>3</sub>SCH<sub>3</sub>, CD<sub>3</sub>SCD<sub>3</sub>, CH<sub>3</sub>SH and CH<sub>3</sub>SSCH<sub>3</sub>. *Journal of Atmospheric Chemistry*, 14(1), 95–108. <https://doi.org/10.1007/BF00115226>
- Jongbloed, U. A., Schauer, A. J., Cole-Dai, J., Larrick, C. G., Porter, W. C., Tashmim, L., et al. (2023). Industrial-era decline in Arctic methanesulfonic acid is offset by increased biogenic sulfate aerosol. *Proceedings of the National Academy of Sciences*, 120(47), e2307587120. <https://doi.org/10.1073/pnas.2307587120>
- Jonson, J. E., Gauss, M., Schulz, M., Jalkanen, J.-P., & Fagerli, H. (2020). Effects of global ship emissions on European air pollution levels. *Atmospheric Chemistry and Physics*, 20(19), 11399–11422. <https://doi.org/10.5194/acp-20-11399-2020>
- Kettle, A. J., Rhee, T. S., von Hobe, M., Poulton, A., Aiken, J., & Andreae, M. O. (2001). Assessing the flux of different volatile sulfur gases from the ocean to the atmosphere. *Journal of Geophysical Research*, 106(D11), 12193–12209. <https://doi.org/10.1029/2000JD900630>
- Kiene, R. P. (1996). Production of methanethiol from dimethylsulfoniopropionate in marine surface waters. *Marine Chemistry*, 54(1–2), 69–83. [https://doi.org/10.1016/0304-4203\(96\)00006-0](https://doi.org/10.1016/0304-4203(96)00006-0)
- Kiene, R. P., & Linn, L. J. (2000). The fate of dissolved dimethylsulfoniopropionate (DMSP) in seawater: Tracer studies using 35S-DMSP. *Geochimica et Cosmochimica Acta*, 64(16), 2797–2810. [https://doi.org/10.1016/S0016-7037\(00\)00399-9](https://doi.org/10.1016/S0016-7037(00)00399-9)
- Kilgour, D. B., Jernigan, C. M., Garmash, O., Aggarwal, S., Zhou, S., Mohr, C., et al. (2025). Cloud processing of dimethyl sulfide (DMS) oxidation products limits sulfur dioxide (SO<sub>2</sub>) and carbonyl sulfide (OCS) production in the eastern North Atlantic marine boundary layer. *Atmospheric Chemistry and Physics*, 25(3), 1931–1947. <https://doi.org/10.5194/acp-25-1931-2025>

- Kilgour, D. B., Jernigan, C. M., Zhou, S., Brito de Azevedo, E., Wang, J., Zawadowicz, M. A., & Bertram, T. H. (2024). Contribution of speciated monoterpenes to secondary aerosol in the Eastern North Atlantic. *ACS EST Air*, *1*(8), 555–566. <https://doi.org/10.1021/acsestair.3c00112>
- Kilgour, D. B., Novak, G. A., Sauer, J. S., Moore, A. N., Dinasquet, J., Amiri, S., et al. (2022). Marine gas-phase sulfur emissions during an induced phytoplankton bloom. *Atmospheric Chemistry and Physics*, *22*(2), 1601–1613. <https://doi.org/10.5194/acp-22-1601-2022>
- Krechmer, J., Lopez-Hilfiker, F., Koss, A., Hutterli, M., Stoermer, C., Deming, B., et al. (2018). Evaluation of a new reagent-ion source and focusing ion–molecule reactor for use in proton-transfer-reaction mass spectrometry. *Analytical Chemistry*, *90*(20), 12011–12018. <https://doi.org/10.1021/acs.analchem.8b02641>
- Lawson, S. J., Law, C. S., Harvey, M. J., Bell, T. G., Walker, C. F., de Bruyn, W. J., & Saltzman, E. S. (2020). Methanethiol, dimethyl sulfide and acetone over biologically productive waters in the southwest Pacific Ocean. *Atmospheric Chemistry and Physics*, *20*(5), 3061–3078. <https://doi.org/10.5194/acp-20-3061-2020>
- Novak, G. A., Kilgour, D. B., Jernigan, C. M., Vermeuel, M. P., & Bertram, T. H. (2022). Oceanic emissions of dimethyl sulfide and methanethiol and their contribution to sulfur dioxide production in the marine atmosphere. *Atmospheric Chemistry and Physics*, *22*(9), 6309–6325. <https://doi.org/10.5194/acp-22-6309-2022>
- Perraud, V., Meinardi, S., Blake, D. R., & Finlayson-Pitts, B. J. (2016). Challenges associated with the sampling and analysis of organosulfur compounds in air using real-time PTR-ToF-MS and offline GC-FID. *Atmospheric Measurement Techniques*, *9*(3), 1325–1340. <https://doi.org/10.5194/amt-9-1325-2016>
- Phillips, D. P., Hopkins, F. E., Bell, T. G., Liss, P. S., Nightingale, P. D., Reeves, C. E., et al. (2021). Air–sea exchange of acetone, acetaldehyde, DMS and isoprene at a UK coastal site. *Atmospheric Chemistry and Physics*, *21*(13), 10111–10132. <https://doi.org/10.5194/acp-21-10111-2021>
- Pimlott, M. A., Pope, R. J., Kerridge, B. J., Latter, B. G., Knappett, D. S., Heard, D. E., et al. (2022). Investigating the global OH radical distribution using steady-state approximations and satellite data. *Atmospheric Chemistry and Physics*, *22*(16), 10467–10488. <https://doi.org/10.5194/acp-22-10467-2022>
- Saunders, S. M., Jenkin, M. E., Derwent, R. G., & Pilling, M. J. (2003). Protocol for the development of the master chemical mechanism, MCM v3 (Part A): Tropospheric degradation of non-aromatic volatile organic compounds. *Atmospheric Chemistry and Physics*, *3*(1), 161–180. <https://doi.org/10.5194/acp-3-161-2003>
- Susaya, J., Kim, K.-H., Phan, N.-T., & Kim, J.-C. (2011). Assessment of reduced sulfur compounds in ambient air as malodor components in an urban area. *Atmospheric Environment*, *45*(20), 3381–3390. <https://doi.org/10.1016/j.atmosenv.2011.03.051>
- Van Roy, W., Van Roozendaal, B., Vigin, L., Van Nieuwenhove, A., Scheldeman, K., Merveille, J.-B., et al. (2023). International maritime regulation decreases sulfur dioxide but increases nitrogen oxide emissions in the North and Baltic Sea. *Commun Earth Environ*, *4*(1), 1–16. <https://doi.org/10.1038/s43247-023-01050-7>
- Williams, T. L., Adams, N. G., & Babcock, L. M. (1998). Selected ion flow tube studies of  $\text{H}_3\text{O}^+(\text{H}_2\text{O})_{0,1}$  reactions with sulfides and thiols. *International Journal of Mass Spectrometry and Ion Processes*, *172*(1–2), 149–159. [https://doi.org/10.1016/S0168-1176\(97\)00081-5](https://doi.org/10.1016/S0168-1176(97)00081-5)
- Wohl, C. (2025). Methanethiol and dimethyl sulfide mole fractions at Weybourne atmospheric observatory, UK summer 2024 [Dataset]. *Zenodo*. <https://doi.org/10.5281/zenodo.14697890>
- Wohl, C., Villamayor, J., Galí, M., Mahajan, A. S., Fernández, R. P., Cuevas, C. A., et al. (2024). Marine emissions of methanethiol increase aerosol cooling in the Southern Ocean. *Science Advances*, *10*(48), 1–9. <https://doi.org/10.1126/sciadv.adq2465>
- Wolfe, G. M., Marvin, M. M., Roberts, S. J., Travis, K. R., & Liao, J. (2016). The Framework for 0-D Atmospheric Modeling (FOAM) v3.1. <https://doi.org/10.5194/gmd-2016-175>
- Woodward-Massey, R., Sommariva, R., Whalley, L. K., Cryer, D. R., Ingham, T., Bloss, W. J., et al. (2023). Radical chemistry and ozone production at a UK coastal receptor site. *Atmospheric Chemistry and Physics*, *23*(22), 14393–14424. <https://doi.org/10.5194/acp-23-14393-2023>
- Yang, M., Beale, R., Smyth, T., & Blomquist, B. (2013). Measurements of OVOC fluxes by eddy covariance using a proton-transfer-reaction mass spectrometer – Method development at a coastal site. *Atmospheric Chemistry and Physics*, *13*(13), 6165–6184. <https://doi.org/10.5194/acp-13-6165-2013>
- Yi, W., Wang, X., He, T., Liu, H., Luo, Z., Lv, Z., & He, K. (2024). High-resolution global shipping emission inventory by Shipping Emission inventory Model (SEIM). <https://doi.org/10.5194/essd-2024-258>